Swirl generation by a directed inlet port of a diesel automotive engine under steady flow conditions

Chapter 59

SWIRL GENERATION BY A DIRECTED INLET PORT OF A DIESEL AUTOMOTIVE ENGINE UNDER STEADY FLOW CONDITIONS

G Hommersom, D J W M Evers and G Huigen (Eindhoven University of Technology, Eindhoven, The Netherlands)

SUMMARY

The steady flow field generated by an eccentrically placed directed inlet port of an automotive engine into an unconfined cylinder is investigated using Laser Doppler Anemometry.

The valve throat velocity profiles at low lift indicate a more or less uniformly distributed outflow at all four locations for all measured components. In the downstream planes two vortices can be observed of about equal strength. No development to a single vortex, i.e. swirling flow, can be distinguished.

The valve throat profiles at highest lift show an outflow that is strongly non–uniform, with the highest velocities in the elongation of the inlet duct. The downstream measurements of the tangential velocities show at the lowest location a tendency towards a swirling flow pattern, though still strongly influenced by the jet issuing from the valve. The measurements at the planes further downstream show the development towards swirling flow.

The axial measurements in the downstream planes near the cylinder wall show a strong jet that rotates with the flow. Especially in the region near the cylinder head, the mass transport takes place close to the cylinder wall. Reverse flow exists in the central region of the cylinder.

The measurements show that the swirl generating capacity of a directional port varies strongly with valve lift. At high lifts the shape of the inlet duct influences the flow field of the valve exit plane. This results in a non uniformly distributed outflow from the valve. Subsequent collision with the cylinder liner causes the development of a single vortex rotation downstream, that is also convected to the head in the reversed flow region. At low lifts, the effect of the inlet port is insignificant. An almost uniform outflow results, and collision with the cylinder liner causes a double vortex in the cylinder and no resultant swirling flow is generated.

Organised by UK and Dutch LDA User Groups, American Society of Mechanical Engineering; sponsored by University College of Swansea; co-sponsored by I Mech E and BHRA.

Laser Anemometry – Proceedings of the 3rd International Conference, pp. 707–721.

NOMENCLATURE

a_0, a_1	= correction factor
f	= frequency
$G(\tau)$	= autocorrelation function
m	= visibility factor
N	= number of data points in the autocorrelation function
n_f	= number of fringes = 13.5 * 2 without frequency shift
p(..)	= probability density function
p	= pressure
r	= radial coordinate cylinder
R	= cylinder radius = 130 mm
r_0	= laser beam radius
s	= fringe separation
v	= mean velocity perpendicular to the laser beam bisector
v_a, v_r, v_t	= velocity components (valve exit)
V_a, V_r, V_t	= velocity components (cylinder)
w	= mean velocity perpendicular to the laser beam plane
z	= axial coordinate cylinder
θ	= angular coordinate cylinder
τ	= correlation delay time
τ_s	= correlator delay time per channel = 50 E–9 sec

1. INTRODUCTION

The inlet valve of an internal combustion engine plays an important role in the gas exchange process and engine performance. The efficiency of the induction process of the engine, i.e. the volumetric efficiency and pumping losses, is significantly influenced by the inlet port behaviour. Also the resulting flow field in the cylinder is determined primarily by the inlet port. In recent years, the details of the inlet port flow field have been investigated with Laser Doppler and Hot Wire anemometers.

Bicen et al.(ref.1), Arcoumanis et al.(ref.2), and El Tahry et al.(ref.3) found that the shape of the velocity profiles in the valve throat region were independent of mass flow rate. Bicen et al.(ref.1) and Arcoumanis et al.(ref.2) reported that the difference in flow pattern for steady and unsteady flow is small in the valve throat region at low engine speeds. El Tahry et al.(ref.4) investigated the flow at higher engine speeds and constant valve lift and observed the same for crank angle regions in which the acceleration of the piston –and hence the acceleration of the inlet duct flow– is small. Since this is the period during which most of the fresh air is admitted, the unsteady effect on the resulting flow pattern in the cylinder is probably small. Stationary flow measurements are thus still attractive because of their simplicity.

The development of the flow field downstream of the valve in a stationary flow rig is investigated by Bicen et al.(ref.1) and Yanneskis et al.(ref.5) for a rotational symmetric geometry, by Coghe et al.(ref.6), Murakami et al.(ref.7) and Brunello et al.(ref.8) for three–dimensional situations with a helical inlet port, and by Brunello et al.(ref.8) for a directed inlet port with a shrouded valve. Cylinder flow fields at unsteady conditions are reported by Bicen et al.(ref.1) for two dimensional geometries, and by Arcoumanis et al. (ref.2) for a helical port.

This present work comprises flow field measurements carried out in a cylinder head with a directed inlet port and an unconfined cylinder. Measurements in the valve exit plane and three downstream cylinder locations under stationary flow conditions provide the relation between the flow field at the valve exit plane and downstream flow development for directed inlet port geometries.

2 LASER DOPPLER ANEMOMETER

The layout of the Laser Doppler Anemometer is shown in fig.1. It is built around a 5 Watt Argon Ion laser. The anemometer is operated in 'dual beam' or 'real fringe' mode: i.e. the laser beam is split into two beams of equal intensity. A TPD type I grating is used as beam splitter. The grating is operated at angular velocities between –100 and 100 Hz, thus providing frequency preshifts of maximum 3.2768 kHz. The two beams are focused by the last lens of the transmitting optics.

The detection optics of the anemometer consists of a photomultiplier, a zoom lens, and a pinhole just before the photomultiplier tube. The receiving optics are placed in off–axis forward scatter mode. This provides a better defined observation volume, i.e. the part of the measuring volume that is observed by the photomultiplier. An additional advantage is that reflections of the laser beams can be avoided.

The entire anemometer is built upon a milling machine bed, which provides a stable platform with accurate X_Y_Z positioning.

The photon correlation technique is used to obtain the velocity information. The autocorrelation function of the scattered light of particles passing through an intersection volume of two Gaussian laser beams is given by Durranni et al.(ref.9):

$$G(\tau) = a_o \int_{-\infty}^{\infty}\int_{-\infty}^{\infty}\left[\exp\left[\frac{-(v^2+w^2)\tau^2}{r_o^{\,2}}\right]\right]\cdot\left[2+m^2\cos\left[\frac{2\pi v\tau}{s}\right]\right]\cdot p(v,w)\,dv\,dw$$

The velocity probability density function cannot easily be extracted from this expression. The Linear Transform as proposed by Staas (ref.11) and further discussed by De Groot (ref.12) is used to obtain the velocity spectrum. The Linear Transform closely resembles a Fourier transform, but the shape of the pedestal i.e. the effect of the exponential attenuation term, is included in the generation function basis. It is assumed that the contribution of the velocity component w perpendicular to the plane of the laser beams is negligible. This implies that integration of the contribution of w becomes independent of the kernel. The spot values of the theoretical autocorrelation function at a number of points N = 96 that are separated by the delay time τ_s = 50E–9 sec satisfy:

$$G(i\cdot\tau_s) = a_3 \sum_{i=1}^{N}\left[\exp\left[\frac{-f_i\cdot j\cdot\tau_s}{n_f}\right]^2\right]\cdot\left[2+m^2\cdot\cos(2\pi f_i j\tau_s)\right]\cdot p_i(f_i) \qquad j = 1 \ldots N$$

The frequency probability density function is then obtained by the Linear Transform. In our experiments, it was not possible to ascertain that the contribution of w to the pedestal was negligible. However, numerical experiments reported by Hommersom (ref.10) showed that the resulting velocity probability distribution was insensitive even for large values of w, because the beam factor was nearly unity.

Photon correlation has the advantage that it requires low scattering intensities, i.e. there is no need for artificial seeding. Thus contamination of the pyrex cylinder is avoided and longer measuring sessions are possible. The disadvantage is that the construction of the autocorrelation function may take up to several minutes, making detection of random unsteadiness of the flow impossible.

The photon pulses of the photomultiplier are amplified by a discriminator to 'binary pulses' that are fed into the MALVERN K7023 digital correlator. Control of the correlation unit and Linear Transform signal processing is provided by the program 'VALIT' (ref.13). The software is written in UCSD Pascal 1.2 and is implemented on a 128 kB Apple IIe microcomputer. The program has command line control. It contains assembly language routines that provide rapid matrix multiplication and readout of the autocorrelation unit, using Direct Memory Access techniques. Complete computation of the velocity distribution, display on the monitor and storage on disk, require approximately 15 sec.

3 EXPERIMENTAL SYSTEM

The cylinder head used originates from a production DAF DKS1160 automotive diesel engine with a directional inlet port. The effect of the cylinder wall is simulated by a pyrex cylinder, which has a diameter equal to the bore of the engine. The cylinder head is placed upside down on a platform that can rotate around a vertical axis and translate vertically (fig.2). The axis of rotation is made to coincide with the measuring cylinder axis when the cylinder velocities are determined. Alternatively, during the measurements in the valve exit plane, the cylinder head is made to revolve around the valve stem centreline. The required valve lift is set by an adjustment screw and the lift is verified with a caliper.

Air is supplied from the main compressed air circuit. Mass flow is monitored with an orifice meter placed far upstream of the inlet pipe. The orifice plate conforms to DIN1952, and is corrected for ambient pressure and temperature assuming air to be an ideal gas. The flow upstream of the cylinder head is conditioned to a fully developed turbulent pipe flow by means of a long straight cylindrical pipe (L/D = 20) with a honeycomb flow straightener positioned at the upstream end. The pressure drop over the cylinder head is determined by measuring the pressure at the connection of the inlet pipe and head. The pressure in the pyrex cylinder is assumed to be uniform and atmospheric.

For the calibration of the anemometer a theodolite is used to measure the angle between the laser beams at the measuring volume with an accuracy of better than 0.1%. Unfortunately the calibration could not be carried out in the pyrex cylinder. Correction for refraction by the cylinder is carried out using the method outlined by Snauwaert (ref.14). This correction is only required for the radial and tangential velocity measurements. An additional source of error is the 'fringe divergence' caused by the non–coinciding positions of beam waist and measuring volume. This error originates from the fact that the 1185 mm transmitting lens is positioned too close to the second lens of the transmitting optics. The maximum relative error is estimated at 1.3% by Hommersom (ref.10). The compressed air circuit provided ample air of nearly constant pressure and temperature. The static pressure upstream of the orifice varied periodically with about 4%. Numerical experiments with the signal processing software by Hommersom (ref.10) proved the accuracy of our implementation of the Linear Transform algorithm to be within 2% provided that the velocity probability density function was not excessively broad.

Initially a 500 mm transmitting lens was used in the cylinder measurements. However, the autocorrelation functions indicated an extremely broad frequency distribution with reference to the frequency window of the correlator. The signal processing software was known to perform poorly in such situations, hence the lens was replaced by the 1185 mm lens. That lens was used throughout the remainder of the cylinder flow measurements and all the valve exit plane measurements. In the tabular summary of measurements (Table 1) the measurements made with the 500 mm lens are marked.

4 EXPERIMENT AND RESULTS

The flow is investigated for valve lifts that are situated in the regions of dimensionless valve lifts as suggested by Bicen et al.(ref.1), where qualitatively different flow patterns have been observed in rotational symmetric flows. In the experiment the mass flow was 275 kg/hr. At some measurement locations in the valve throat region, additional measurements were carried out with mass flows of 135 and 443 kg/hr to investigate the influence of mass flow on the flow field. Higher mass flows could not be reached in the described apparatus.

Velocities are determined on the valve periphery at four positions of the valve circumference (fig.3). Radial and axial velocity components with respect to the valve geometry are measured. Downstream, in the cylinder, measurements were carried out at three axial planes along eight radii spaced at 45^0 intervals. Table 1 summarizes the experiments.

The measurements reproduce well despite the scatter of data in some locations. This scatter is found near regions of steep velocity gradients and is attributed to positional inaccuracy of the anemometer between two subsequent runs. It is very difficult to obtain better than ± 0.5 mm spatial accuracy, which, in several regions in the flow domain, includes the entire width of the gradient. An additional contribution to the scatter of data is the probable non–stationary nature of the flow downstream of the valve. The noise of the cylinder flow suggested the presence of flow oscillation. The cause of this non–stationary behaviour of the cylinder flow is thought to originate from vortex shedding from the valve. The use of the correlator, with its comparatively long signal intake period, precludes the detection of such non–stationary behaviour other than by an exceptionally broad frequency (= velocity) spectrum. These broad frequency distributions were observed, and necessitated the replacement of the transmitting lens of the anemometer to improve the results of the signal processing software (see par.3).

4.1 Flow at 5 mm valve lift

The measurements in the valve throat region (fig.4) show axial and radial velocity profiles of a jet that are nearly independent on the position along the valve circumference. The angle of the flow, with respect to the cylinder axis, is 20^0 and nearly uniform over the jet height at all measurement locations. Separation near the cylinder head is only present at location III. Here, the jet angle increases to 24^0.

The measurements of the tangential component of the velocity further downstream in the cylinder show clearly a dual vortex flow at all downstream locations (fig.5). The position of the centres of the two vortices does not change with z–location. The symmetry of the dual vortex flow can readily be seen in fig.6 which shows the tangential velocity as function of angular position for three radii. The axis of symmetry coincides approximately with the line passing through the valve centre and the cylinder centre ($\theta \approx 70^0$ and $\theta \approx 250^0$).

The axial velocity profiles show the reversed flow region in the centres of both vortices (fig.7). The downstream mass transport effectively takes place close to the cylinder walls. High axial velocities are also found in the cylinder centre, mass transport, however, is small because of the small cross–sectional area. The high axial velocities near the wall are initially located at the entire circumference of the cylinder. At z = 130 axial velocity peaks are situated at $\theta \approx 45^0$ and $\theta \approx 90$, roughly symmetrically with respect to the geometrical symmetry axis at $\theta = 70^0$

4.2 Flow at 9 mm valve lift

The measurements in the valve throat show that the axial and radial velocity profiles are increasingly dependent on position along the valve circumference (fig.8). Higher velocities and smaller separation regions exist near the head for locations approaching the elongation of the inlet channel direction. A large separation zone is found opposite this direction. Significant separation occurs at right angles with the port centreline. The jet issues at $\approx 30^0$ in the elongation of the port, revolving more towards the head with increasing angle from this direction. The jet issues at $\approx 24^0$ in the opposite direction III. The velocities are much lower compared to the 5 mm lift situation.

At one diameter downstream, the flow in the cylinder again shows a dual vortex structure. At z = 32 mm, the effect of the valve jet on the tangential velocity component prevents a clear flow pattern. At z = 80 mm, the influence of the jet diminishes, and a flow pattern with two vortices of unequal strength is seen. This develops towards a symmetrical dual vortex flow further downstream (fig.9). This phenomenon is illustrated by fig.10 which shows the tangential velocity as a function of angular position for three radii.

The axial velocity profiles in the cylinder exhibit phenomena consistent with the above described tangential structure. The area of the strong vortex at low z also shows flow

reversal, which is nearly absent in the region of the weaker vortex. At higher z, the axial profile turns towards a symmetrical situation of the 5 mm flow pattern.

4.3 Flow at 12.7 mm valve lift

The velocities in the valve throat region show an even greater dependence on position along the valve circumference. Flow separation is present at all locations, except position IV (fig.11). The jet issues at $\approx 31^0$ from the valve opening at position I. At the other locations the jet angle varies strongly over the jet. Large separation zones are present at location II and III. The peak velocity magnitudes near the valve disk have not decreased compared to the 9 mm flow.

The double vortex structure of the cylinder flow has disappeared completely at all downstream measuring planes. At the z = 32 mm plane, the effect of the jet issuing from the valve is visible in the tangential velocity distribution as peaks on the velocity distribution. Three different vortical structures may be identified (fig.12). The central region of the cylinder revolves as a solid body. A strong jet close to the wall penetrates over almost the entire cylinder circumference. It originates from the valve exit section in the elongation of the inlet channel. This strong jet forces the jet section issuing from position III of the valve more inward. A solid body rotation stabilizes further downstream as the jet effect decays. At z = 130 mm the swirling motion is completely established. The axial velocity conforms to the tangential flow pattern with a large reversed flow region in the centre. A single axial velocity peak revolves with the swirl motion downstream(fig.13).

4.4 The effect of mass flow

Measurements were carried out at position II with varying mass flow. This position was taken, because it exhibited a separated flow at the larger lifts, and sensitivity to mass flow effects was assumed to be high. Fig.14 shows that at this location the effect of mass flow variation is negligible.

5 DISCUSSION

The measurements in the valve throat show that with increasing valve lift the velocity distribution and mass flow tend to become more dependent on the position at the valve disc circumference. This is shown in diagram 15. The maximum values of the mass flux are reached in the elongation of the inlet port, the minimum values opposite that point. The formation and growth of regions with separated flow from the cylinder head boundary at the various measuring points conform with the above observation. The interaction of the valve jet and the cylinder wall causes the development of vortices in the cylinder. It is the asymmetry of flow field in the valve exit plane which causes swirl to develop, otherwise the incoming momentum is symmetrically distributed with respect to the line connecting the valve and cylinder centres.

The flow field development in the valve exit plane can be explained by analyzing the global pressure fields in the inlet port. Two principal factors are involved: the overall pressure drop over the cylinder head, and the radial pressure gradients induced by the curve of the inlet port just upstream of the valve throat. The overall pressure drop is measured and Table 2 lists the values. The pressure gradient in the curve that provides the centrifugal acceleration is given by:

$$\frac{dp}{dr} = \frac{\rho V^2}{R}$$

Substituting typical values of the inlet port and the local bulk velocity yields the radial pressure difference in the curve (table 2). The increase of the pressure drop across the cylinder head from 1.8 kPa at 12.7 mm valve lift to 4.5 kPa at 5 mm lift is concentrated in the valve throat region. It undoes the curvature induced pressure difference and establishes the mass flux independence on circumferential position of the valve. At higher lifts both pressure gradients are of the same order, and some influence of the curvature on the valve exit flow is expected. The observed independence of valve throat velocity profiles also follows from this analysis, since both pressure gradients are proportional to the dynamic pressure of the flow.

An alternative explanation for these phenomena may be found in the geometry of the inlet channel in relation to the valve exit geometry: more especially in the distribution of cross–sectional area along the length of the channel. The smallest cross–section of the port is located near the point of entry of the valve stem and amounts to $\approx$15E–4 m^2. The smallest cross–sectional area of the valve throat is for the 5 mm valve lift 7.1E–4 m^2, increasing to

13E–4 m^2 for 9 mm lift, to become 18.6E–4 m^2 at 12.7 mm lift. This shows that the narrowest cross–section of the entire system –the determining factor for the mass flow through the inlet as a whole– moves from the valve throat upstream to the narrowest port section. At the lowest lift the mass flux is determined by the valve exit cross–section. This implies a rotational symmetric jet issuing from the valve exit plane, hardly influenced by upstream port geometry, or by the presence of the cylinder wall. The air –incompressible as it is– accelerates towards the narrowest cross–section to satisfy continuity conditions. Any separation zone is rapidly quenched by the negative pressure gradient that establishes this acceleration. If the major restriction of the inlet moves upstream, the air is retarded by the positive pressure gradient before it reaches the valve exit region, and geometry induced separation is promoted. The adverse pressure gradient is largest at the lower boundary of the port, hence position III is most sensitive to flow separation. The influence of the cylinder liner on the velocity distribution in the valve exit plane cannot be established from the presented measurements.

The flow generated by the valve–port at low lift with its double vortex structure is similar to the flow structure reported by Arcoumanis et al.(ref.15), though the vortices revolve in opposite direction. The difference in vortex rotation is not explained. Oil traces on the cylinder surface of the stationary model support the direction of rotation reported here. Arcoumanis et al.(ref.15) measured the flow in a motored engine model with a straight inlet duct parallel to the cylinder axis that was located eccentrically in the cylinder head. This supports the argument of the above paragraph that for the low lift situation of our experiment the upstream geometrical influence is lost. The double vortex flow was found to collapse at the end of the compression stroke of the model engine. The stabilization that occurs under stationary conditions further downstream is hence an effect that disappears in the non–stationary engine situation.

The flow situation in the cylinder at 9 mm valve lift with its two vortices of unequal strength develops in the stationary situation to the double vortex structure of the low valve lift situation. Arcoumanis et al.(ref.15) report an analogous flow field, created by inducing rotation in the inlet flow by means of guide vanes, which developed to a single vortex flow with an eccentric and swirling core. In the stationary situation of our experiment, circulation of the larger vortex is transported upstream in the wake of the valve. The smaller vortex does not lose momentum by reverse flow convection. Hence, both vortices develop towards equal strength further downstream. In the engine model of Arcoumanis et al.(ref.15) this downstream development is prevented by the piston.

The cylinder flow at 12.7 mm valve lift is less complicated in the downstream measuring planes than at the lower lifts. Close to the cylinder head, however, the flow is still complicated because of the influence of the valve jet.The central region with its solid body rotation at z = 32 mm is caused by vorticity transported from the downstream regions by the reversed flow in the valve wake.

6 CONCLUSIONS

The stationary simulation of the induction flow through a poppet valve into the cylinder of an engine leads to an extremely complicated three dimensional flow field. In the case of a directional inlet port, interaction of the annular jet from the valve exit with the cylinder wall leads to vortex formation in the cylinder flow.

The effect of the inlet channel orientation is not significant at low lift but becomes progressively important at larger lifts. This is accompanied by an increasingly non–symmetrical annular jet and a shift of the narrowest cross–section of the inlet port from the valve exit to a more upstream location.

The swirl generating capacity of a directional port, i.e its capacity to generate a single vortex flow, depends on the location of the smallest cross–section of the inlet channel.

It is concluded that the development of the stationary flow in streamwise direction cannot be taken as an indication of the development of the non–stationary flow in the cylinder with a moving piston assembly.

7 LITERATURE

1 Bicen, A.F., Vafides, C., Whitelaw, J.H.: "Steady and unsteady airflow through the intake valve of a reciprocating engine". J. Fluids Eng., Vol.107, Sept. 1985.

2 Arcoumanis, C., Vafides, C., Whitelaw, J.H.: "Valve and in–cylinder flow generated by a helical port in a production Diesel engine". J.Fluids Eng., Vol.109, Dec 1987.

3 El Tahry, S.H., Khalighi, B., Kuziak Jr, W.R.: "Measured steady flow velocity distributions around a valve/seat annulus". Soc.Auto.Eng.Paper 860462, 1986.

4 El Tahry, S.H., Khalighi, B., Kuziak Jr, W.R.: "Unsteady flow velocity measurements around an intake valve of a reciprocating engine". Soc.Auto.Eng.Paper 870593, 1987.

5 Yanneskis, M., Tindal, M.J.: "A method of investigating flows in inlet ports of complex shape". Proc.Int.Conf."Combustion in engines –Technology and applications", Paper C62/88, Inst.Mech.Eng.Publications, London 1988.

6 Coghe, A., Gamma, F., Mauri, M., Brunello, G., Calderini, F.,Antoni, L.F.: "In–cylinder air motion measurements by laser velocimetry under steady–state flow conditions". Soc.Auto.Eng.Paper 850123, 1985

7 Murakami, A., Hishida, K., Arai, H., Hiroyasu, K., Kajiyama., K.: "Steady test of in–cylinder air motion of engine with LDV". Bull.J.S.M.E., Vol.29, No.258, 1986

8 Brunello, G., Coghe, A., Gamma, F.: "Analysis of in–cylinder air motion and turbulence structure under steady flow conditions". Proc.3rd.Int.Symp.Laser Anemometry in Fluid Mechanics, Lisbon, 1986.

9 Durranni, T.S., Greated, C.A.: "Laser systems in flow measurement". Plenum Press, New York, 1977.

10 Hommersom G.: "The application of computational fluid dynamics to induction flow in Diesel engine–like geometries". Ph.D Thesis, Eindhoven University of Technology. In preparation.

11 Staas, F.A.: On–line data reduction of the Doppler difference autocorrelation function". Proc.Int.Conf. on Laser Anemometry, Manchester, BHRA, 1985.

12 De Groot, P.J.: "Usefullness of several analysing methods for photon–correlation LDA data". Proc.Int.Conf. on Laser Anemometry, Manchester, BHRA, 1985.

13 Hommersom, G., Koene, F.G.H., Jaasma, S.A.M.: "VALIT, een signaalverwerkings programma voor Laser Doppler Anemometrie". Rep.WV157–027, Eindhoven University of Technology, Mech.Eng.Dept, 1989.

14 Snauwaert, P.: "Studie van de swirl beweging bij direkte injektie Diesel motoren d.m.v. Laser Doppler Anemometrie". Ph.D Thesis, State University, Gent, 1984

15 Arcoumanis, C., Bicen, A.F., Vafides, C., Whitelaw, J.H.: "Three–dimensional flow field in four–stroke model engines". Soc.Auto.Eng.Paper 841360, 1984.

Table 1: Measurements

Direction velocity	Valve lift 5 mm	Valve lift 9 mm	Valve lift 12.7 mm
RADIAL	Throat: I m=272 II m=272, m=135 III m=272 IV m=272	Throat: I m=272 II m=272, m=135 III m=272 IV m=272	Throat: I m=272 II m=272, m=135, 443 III m=272 IV m=272
	Cylin. R1–8 m=275 (f500) z=32,130	Cylin. R1–8 m=275 (f500) z=32,80,130	Cylin. R1–8 m=275 z=32,80,130
AXIAL	Throat: I m=272 II m=272, m=135 III m=272 IV m=272	Throat: I m=272 II m=272, m=135 III m=272 IV m=272	Throat: I m=272 II m=272, m=135, 443 III m=272 IV m=272
	Cylin. R1–8 m=275 (f500) z=32,80,130	Cylin. R1–8 m=275 (f500) z=32,80,130	Cylin. R1–8 m=275 z=32,80,130
TANGENTIAL	Cylin. R1–8 m=275 (f500) z=32,80,130	Cylin. R1–8 m=275 z=32,80,130	Cylin. R1–8 m=275 z=32,80,130

Table 2: Pressure differences (kPa)
mass flow: 275 kg/hr

	Valve lift 5 mm	Valve lift 9 mm	Valve lift 12.7 mm
ΔP (head)	4.5	2.0	1.8
ΔP (curve)	0.62	0.62	0.62

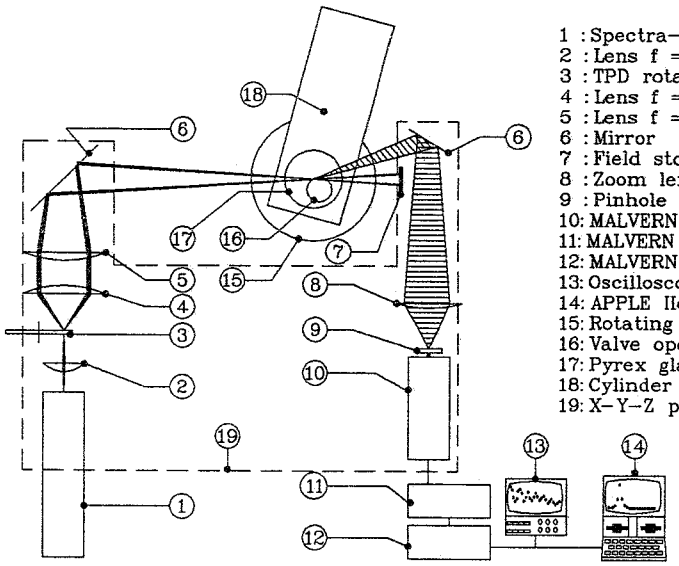

1 : Spectra–Physics Ar–Ion Laser
2 : Lens f = 200 mm
3 : TPD rotating diffraction grating
4 : Lens f = 200 mm
5 : Lens f = 1185 mm
6 : Mirror
7 : Field stop
8 : Zoom lens f = 80 – 240 mm
9 : Pinhole and filter
10: MALVERN RF313 Photomultiplier
11: MALVERN K7023 Correlator controller
12: MALVERN K7023 Correlator store
13: Oscilloscope
14: APPLE IIe computer
15: Rotating plateau
16: Valve opening
17: Pyrex glass cylinder
18: Cylinder head
19: X–Y–Z plateau

FIG.1: ANEMOMETER AND CYLINDER HEAD

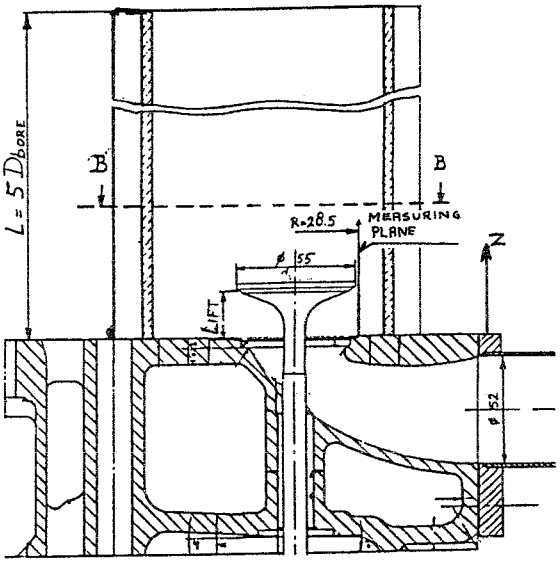

FIG: 2: CROSS–SECTION OF THE INLET PORT

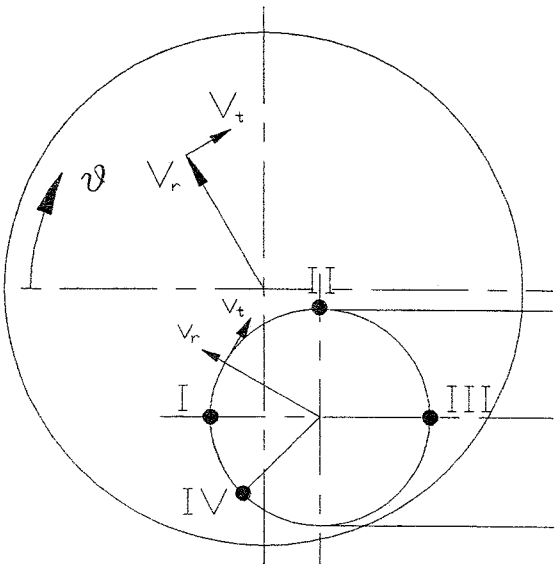

FIG. 3: PLAN OF THE INLET PORT

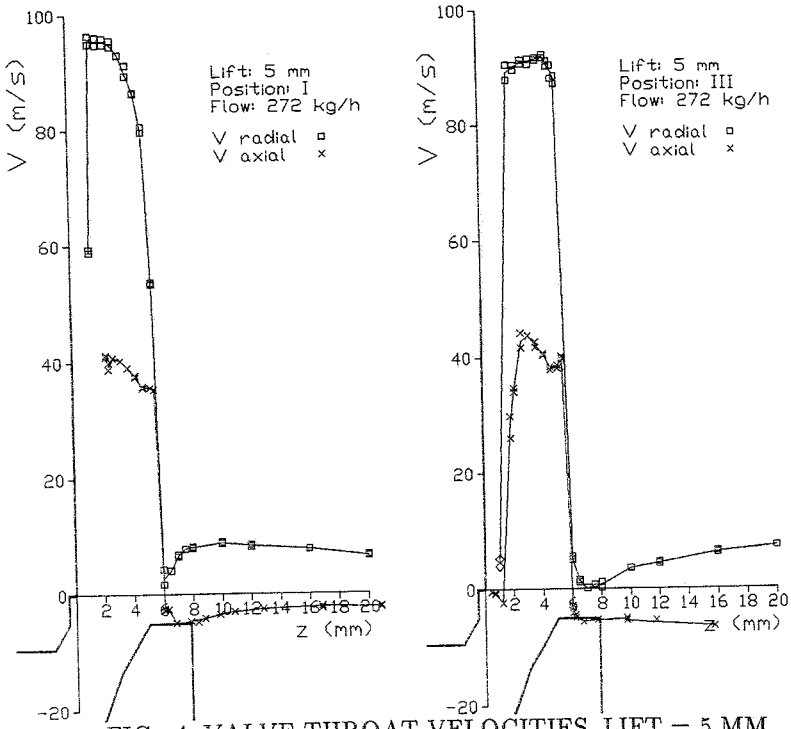

FIG. 4: VALVE THROAT VELOCITIES. LIFT = 5 MM.

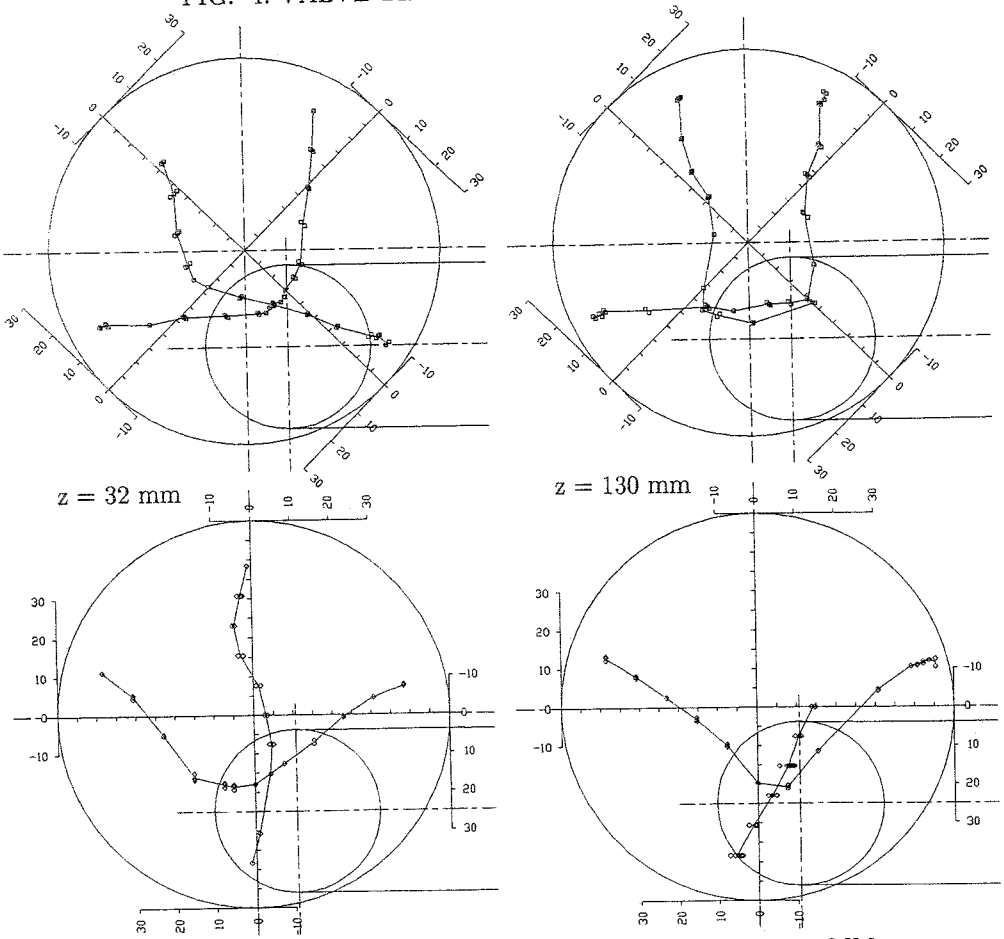

FIG. 5: CYLINDER TANGENTIAL VELOCITIES. LIFT = 5 MM.

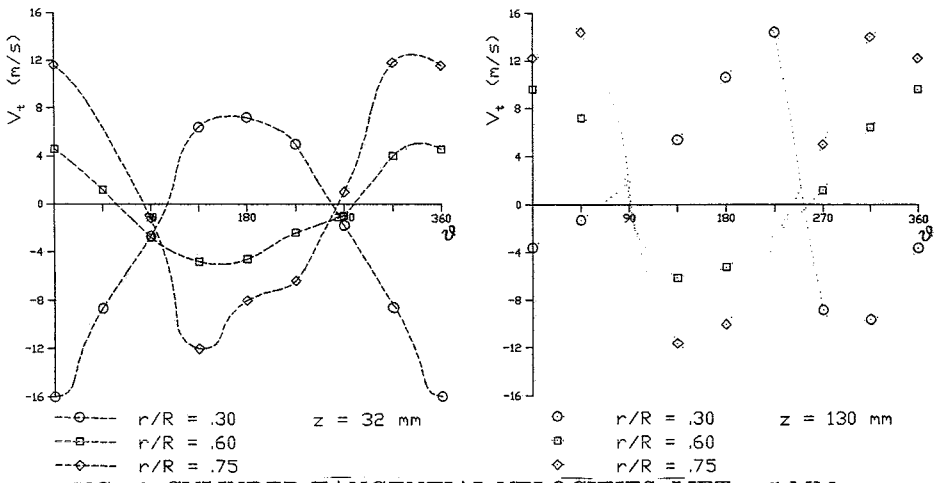

FIG. 6: CYLINDER TANGENTIAL VELOCITIES. LIFT = 5 MM.

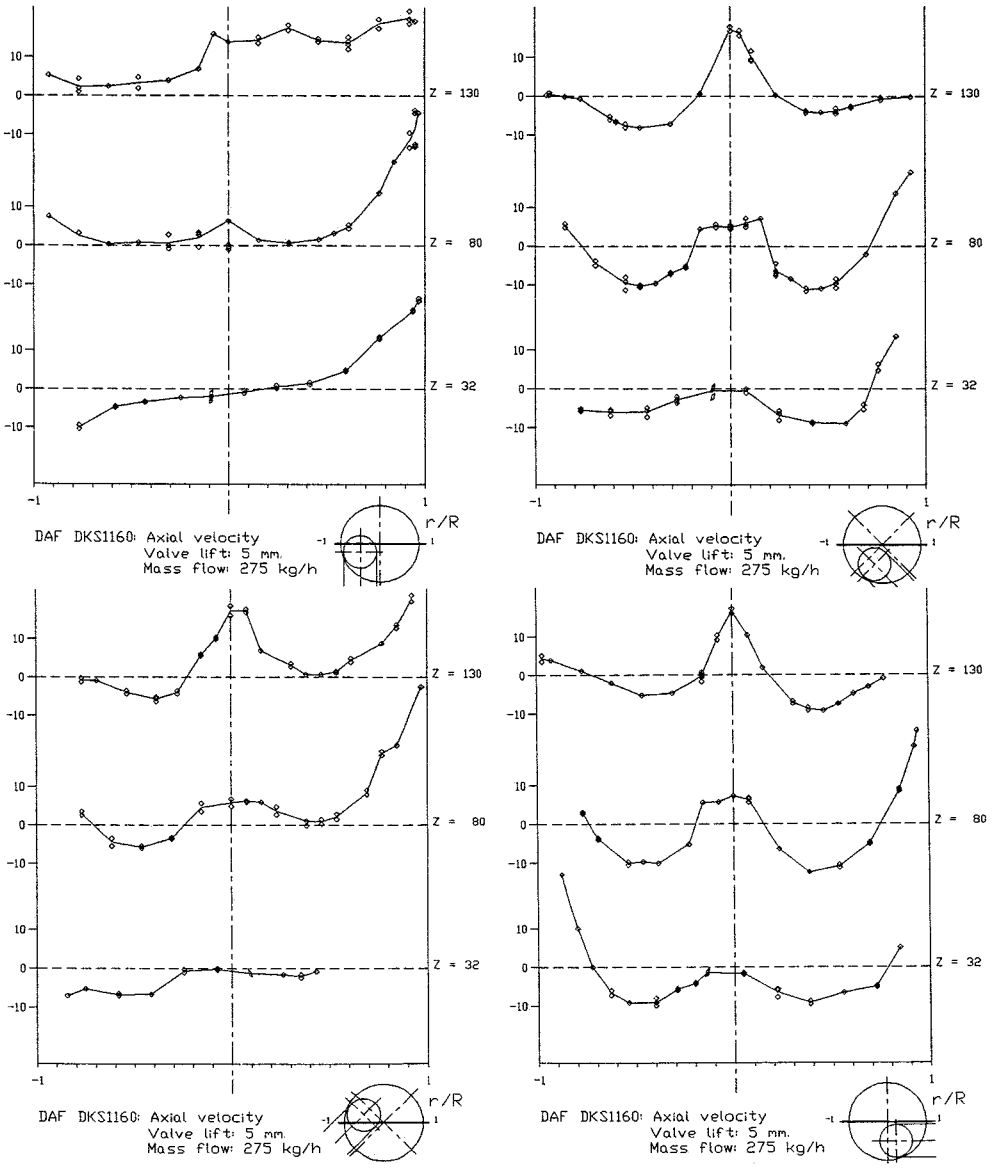

FIG. 7: CYLINDER AXIAL VELOCITIES. LIFT = 5 MM.

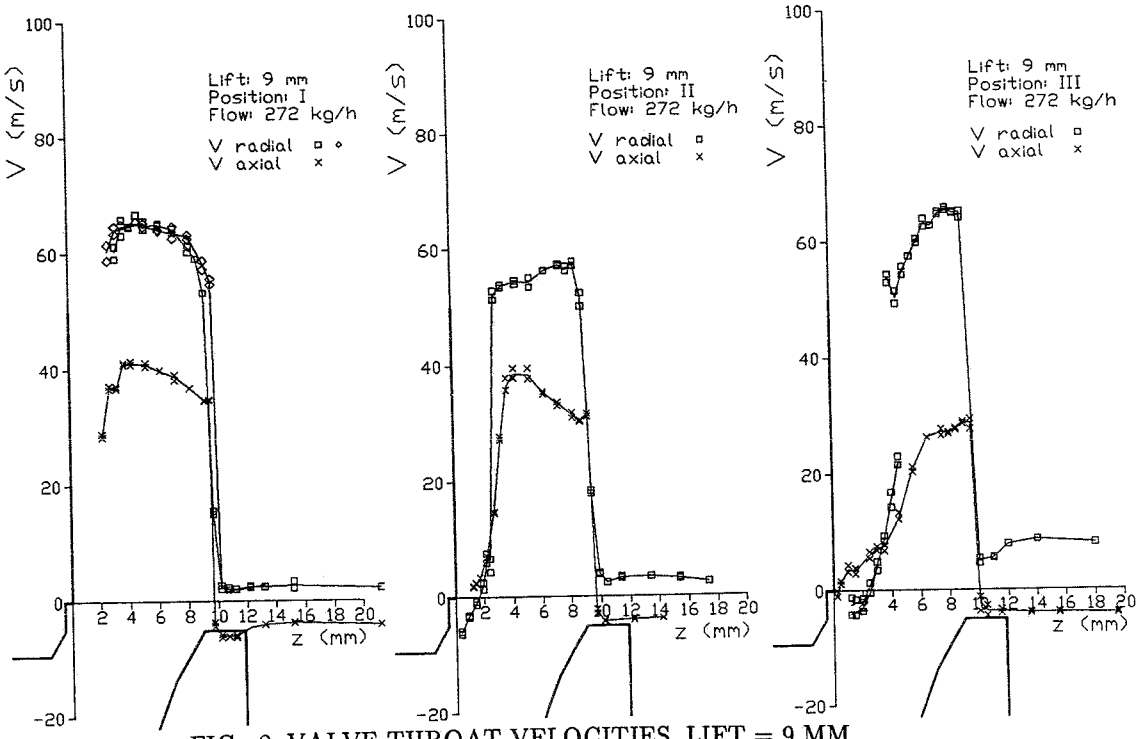

FIG. 8: VALVE THROAT VELOCITIES. LIFT = 9 MM.

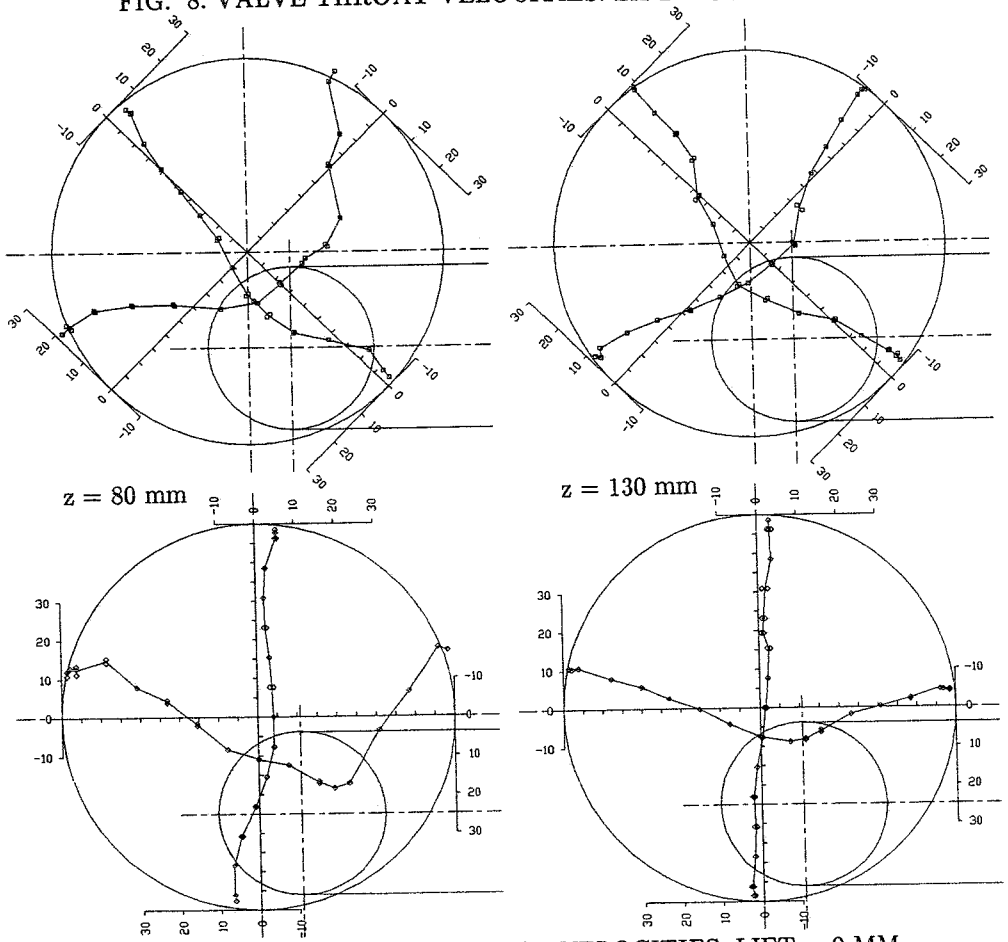

FIG. 9: CYLINDER TANGENTIAL VELOCITIES. LIFT = 9 MM.

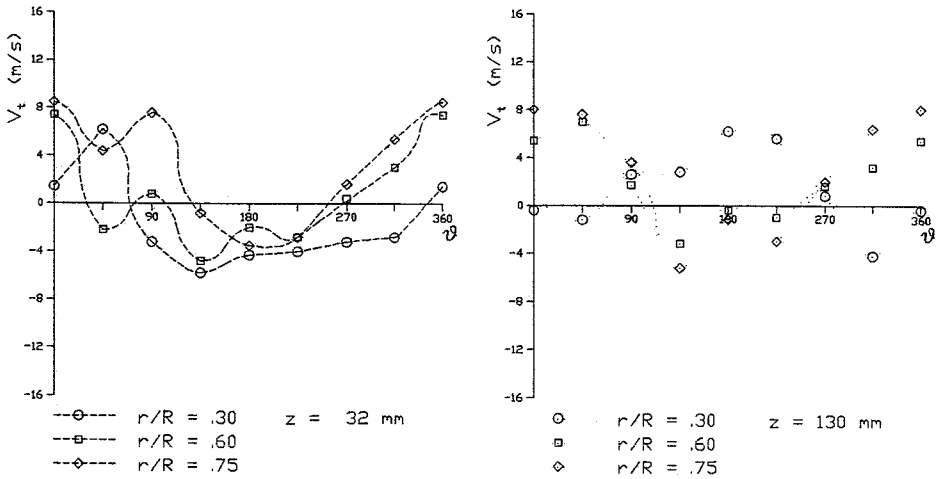

FIG. 10: CYLINDER TANGENTIAL VELOCITIES. LIFT = 9 MM.

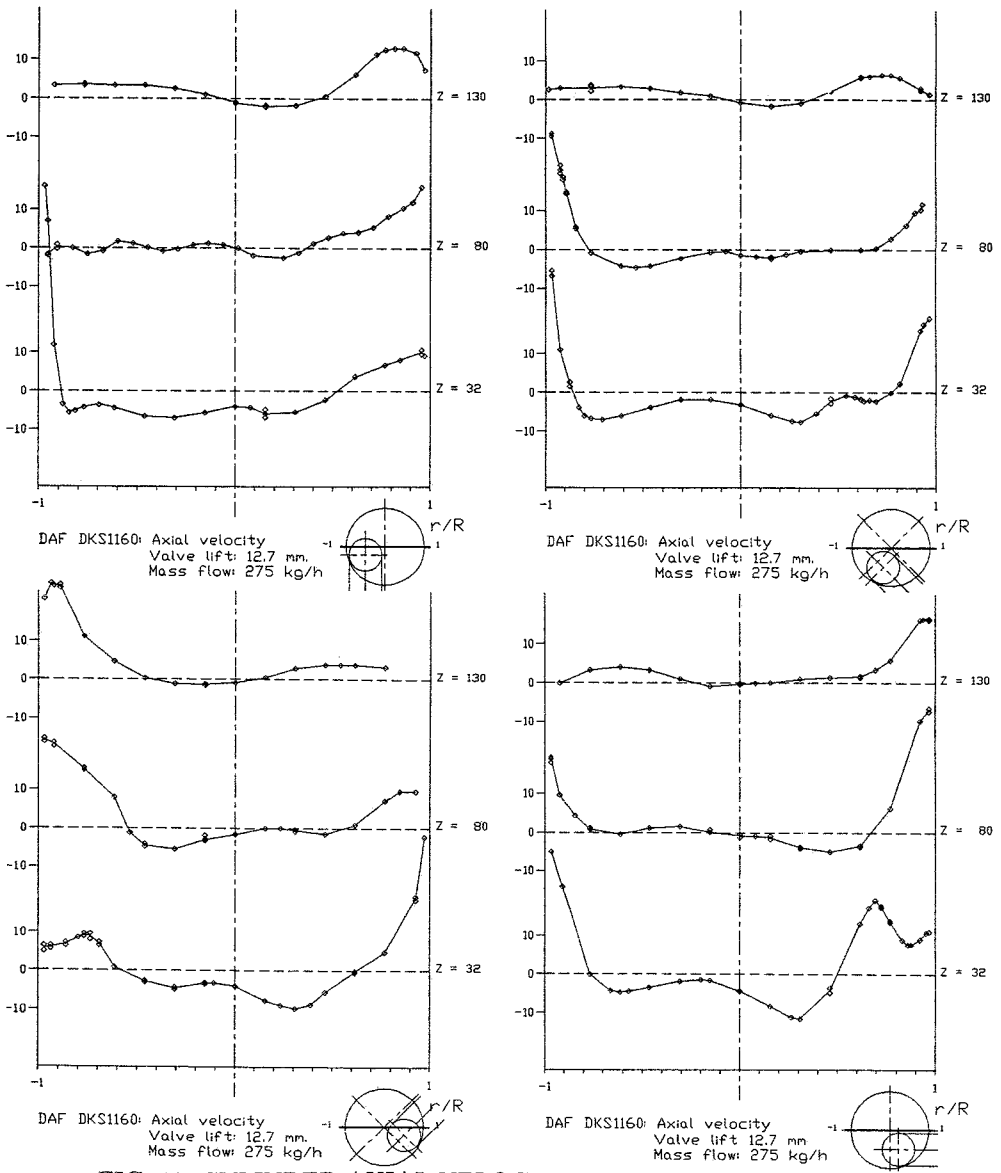

FIG. 13: CYLINDER AXIAL VELOCITIES. LIFT = 12.7 MM.

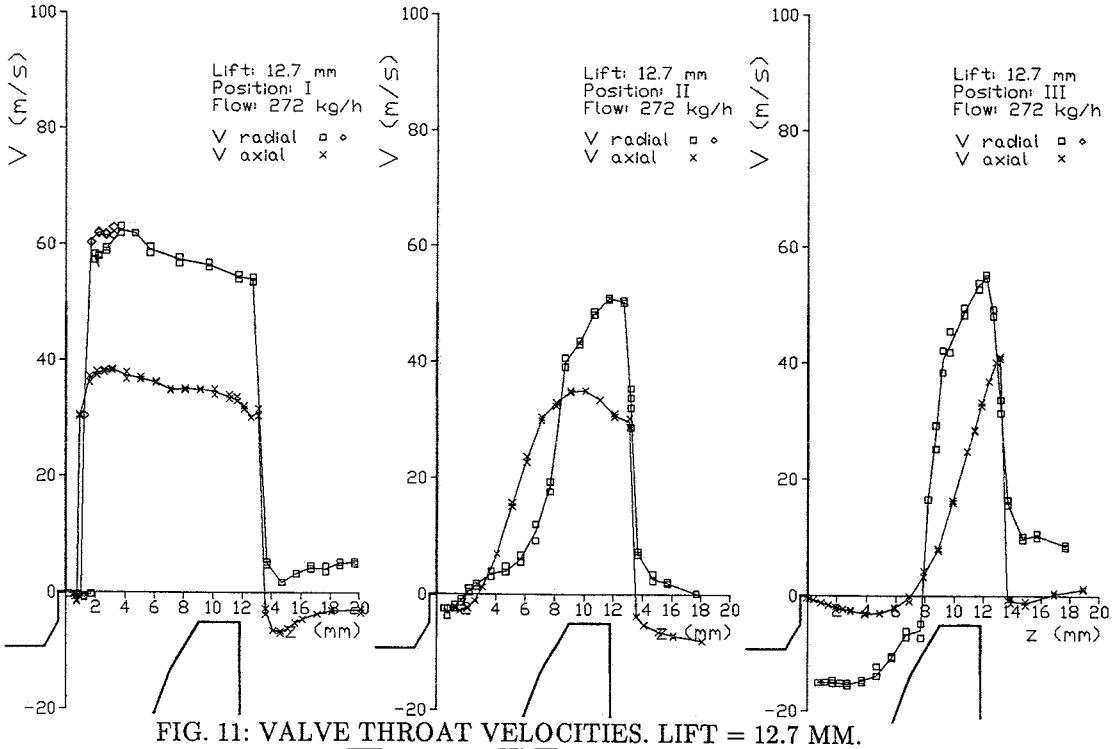

FIG. 11: VALVE THROAT VELOCITIES. LIFT = 12.7 MM.

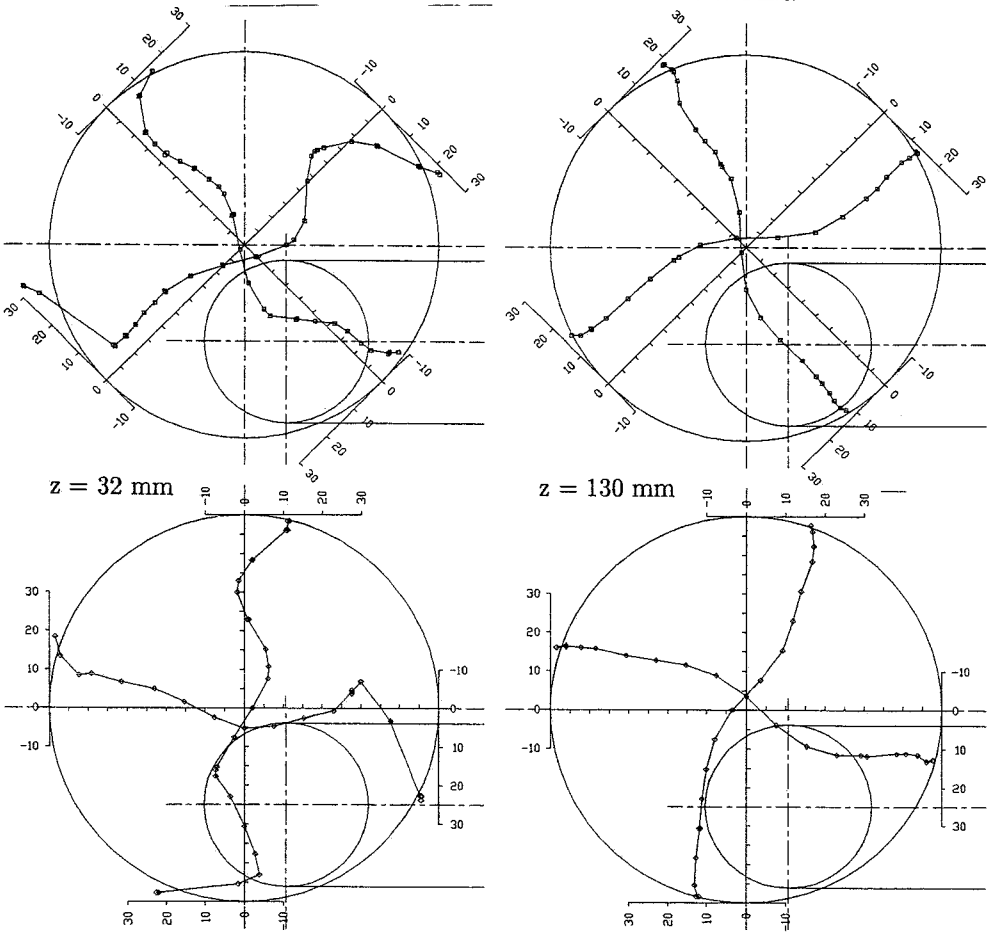

FIG. 12: CYLINDER TANGENTIAL VELOCITIES. LIFT = 12.7 MM.

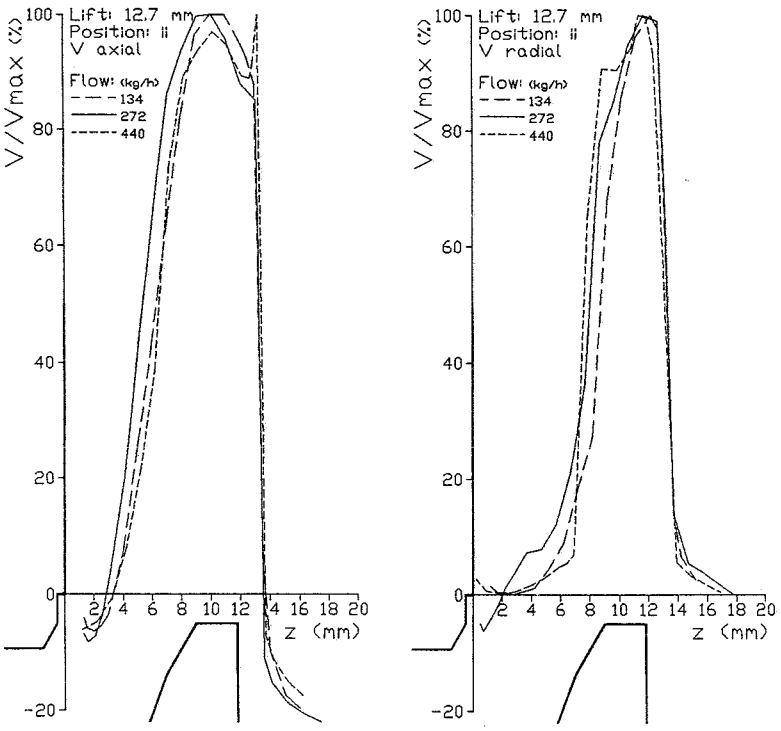

FIG.14: VALVE THROAT VELOCITIES.

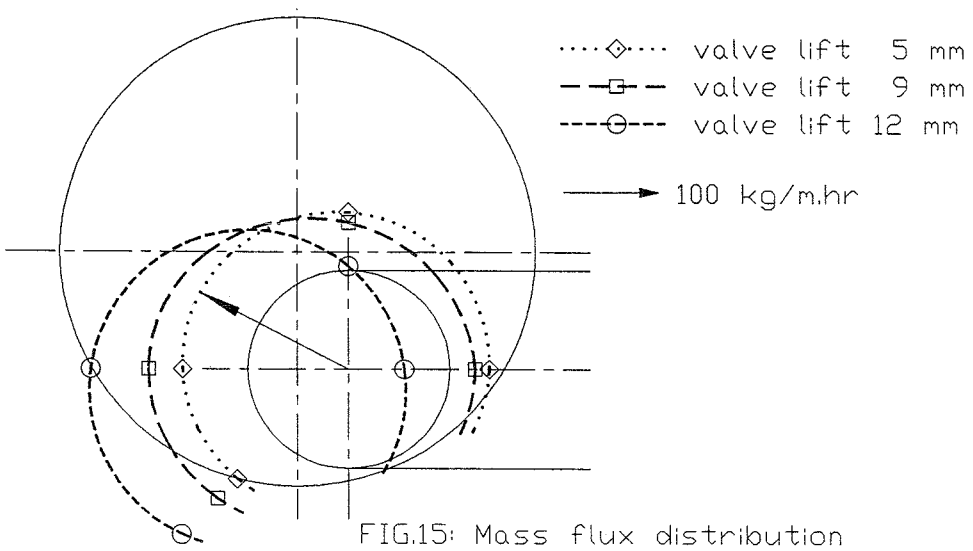

FIG.15: Mass flux distribution